Large-eddy simulation of fuel effect on lean blow-out in gas turbines

By L. Esclapez, P. C. Ma AND M. Ihme

1. Motivation and objectives

Motivated by the need for fuel-security and rising concerns regarding the impact of pollutant emissions on the environment, significant research efforts have been made on utilizing alternative fuels for aviation (Maurice *et al.* 2001; Edwards 2007; Blakey *et al.* 2011). Due to the long life of commercial aircraft and the required compatibility with the present supply infrastructures, research efforts focus on the development of 'drop-in" fuels which can be used in the existing fleet (Blakey *et al.* 2011). The certification of candidate fuels then requires to demonstrate the capability of the fuel to ensure safe and reliable ignition at altitude and the stable combustion at very lean combustions (ASTM 2014). In particular, the lean blow-out (LBO) performance is especially important due to recent emphasis on lean-combustion strategies for emission reduction.

Most of the early work on LBO focused on bluff-body flameholder configurations (Ballal & Lefebvre 1979). Due to limited optical access and absence of high-speed imaging, experiments were used to support the development of semi-empirical correlations to relate LBO-criteria to equivalence ratio and other operating conditions. The review by Shanbhogue *et al.* (2009) describes the blow-off mechanism as a two-stage stochastic process: as the overall equivalence ratio approaches the LBO-limit local flame extinction occurrences increase, and very near blow-off the flame behavior is mainly dominated by auto-ignition with successive extinction and re-ignition of the recirculation bubble. However, studies of LBO-limits in swirl-stabilized burners, relevant for aviation gas turbines, are limited. Correlations have been developed for gas turbine combustors (Lefebvre 1985) including the effect of swirl (Feikema *et al.* 1990), combustor design (Ateshkadi *et al.* 2000) and two-phase flow. Indeed, studies in academic swirling burners (Marinov *et al.* 2012; Cavaliere *et al.* 2013) emphasized the sensitivity of the LBO-behavior of liquid fueled combustor. Recently, high-speed imaging of OH^* (Muruganandam & Seitzman 2005) and simultaneous high-speed stereo-PIV and OH-PLIF measurements (Stöhr *et al.* 2011) revealed that the LBO-behavior in swirled combustors is closely related to the temperature of the recirculation zone and the flame root dynamics. Blow-out was shown to have several precursor events, in which cold gases were captured by the recirculation zone, resulting in a reduction of heat release and a change in the flame shape. LBO was found to occurs when the flame root was extinguished by its interaction with the precessing-vortex core (PVC) for a duration that exceeds a PVC-period. Several studies have been performed to quatify the effect of fuel properties on the LBO-limit in model combustors (Moses & Naegeli 1979; Lefebvre 1985; Lieuwen *et al.* 2008). These studies indicate the beneficial effect of lowering the flash point and the adverse effect of an increase in viscosity on the LBO-performance.

Since LBO is a stochastic process, comparatively few attempts have been made to evaluate the blow-out behavior through numerical simulations even though large eddy simulations (LES) have been proven relevant for the study of transient processes such

as thermo-acoustic instabilities (Selle *et al.* 2004) and gas turbine ignition (Esclapez *et al.* 2015). LES of blow-out in a swirl-stabilized spray flame (Cavaliere *et al.* 2013) was performed by Tyliszczak *et al.* (2014) using the LES-CMC model. LES was shown to be able to capture the local flame extinction and the subsequent blow-out process following a step increase of the air mass flow rate.

The objectives of the present work is to investigate the sensitivity of LBO triggered by fuel depletion to fuel properties in a well controlled but realistic referee-combustor using LES. To this end, three fuels are selected and the effect of their properties on relevant physicochemical processes is analyzed. Then, two fuels are used to perform transient simulations of LBO induced by a progressive reduction of the fuel mass flow rate. The numerical setup is described in Section 2, followed by a description and an analysis of three selected fuels in Section 3. Section 4 presents numerical results of LBO and a description of the flame dynamics close to blow-out. The paper finishes with conclusions.

2. Large-eddy simulation setup

2.1. *Configuration*

The referee-rig combustor studied in this work is installed at Air Force Research Laboratory (AFRL) and is designed to reproduce the main features of a realistic gas turbine combustion chamber. The combustor is operated in a pressurized vessel with large optical access to allow direct visualization of the flame. The four main components of the experimental configuration are included in the simulation: the large pressurized plenum, the complex injection system, the combustion chamber and the exhaust plenum. As shown in Figure 1 the injection system comprises two outer axial swirlers and an inner radial swirler with a pressure-swirl atomizer nested in the center. The combustor liner consists of multi-perforated plates and 2 rows of dilution hole are located at two axial positions. The domain is discretized using 20 million elements with regular hexahedral elements inside the combustor and tetrahedral elements are used to represent a portion of the injector geometry. The characteristic mesh size ranges from 0.15 mm in the swirlers passages to 0.9 mm in the downstream part of the combustor.

Near blow-out condition, the burner is fed with air at 394 K and a relative pressure drop of 3% at a total pressure of 2.07 atms corresponding to an air mass flow rate of 392 g/s. An initial fuel mass flow rate of 2.5 g/s at 322 K is supplied though the pressure-swirl atomizer, corresponding to an overall equivalence ratio $\phi = 0.1$.

2.2. *Computational parameters*

Simulations are performed with the low-Mach LES-solver Vida†. The instantaneous Favre-averaged conservation equations for mass and momentum are solved on the LES grid with a fourth/second-order accurate spacial discretization scheme on regular and unstructured meshes, respectively. A second-order predictor-corrector scheme is used for temporal integration. Turbulent subgrid stresses are modeled with the eddy-viscosity model of Vreman (2004). Walls are considered adiabatic non-slip and the effusive cooling is modeled through a homogeneous approach in which the effusive gas-phase velocity is determined from the experimentally measured mass flow rates.

The spray is modeled using a Lagrangian approach where the droplet motion is described by the Basset-Boussinesq-Oseen (BBO) equation and the evaporation rate is based on equilibrium calculations of isolated droplets (Miller *et al.* 2001). Secondary

† http://www.cascadetechnologies.com/pdf/VIDA.pdf

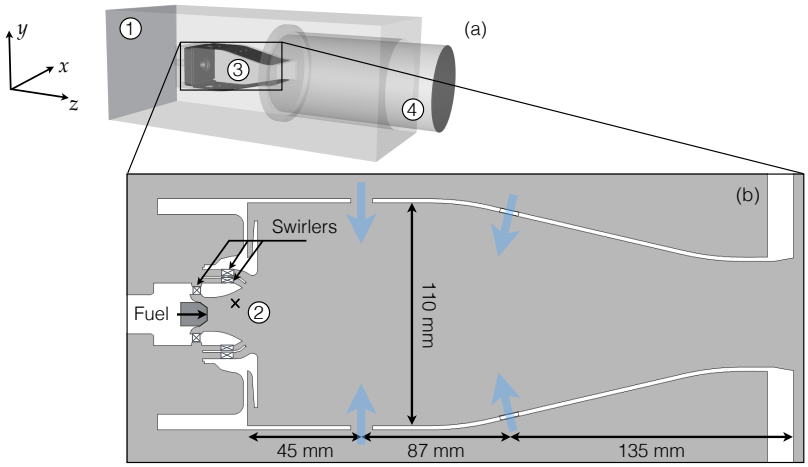

FIGURE 1. Computational domain (a) and details of the injection system in a x-normal central cut plane (b). Main components: 1. Pressurized plenum, 2. Injection system, 3. Combustion chamber, 4. Exhaust plenum.

droplet break-up of Lagrangian particles into smaller drops was found to be important since the low injection velocity and the high flow velocity issued by the swirler result in a large droplet Weber number (ranging between 2 and 20). Secondary breakup is modeled by a stochastic approach where the radius of the droplets is assumed to be a time-dependent stochastic variable with a given initial-size distribution (Apte *et al.* 2003). The critical Weber number is set to a numerical value of 6 based on experimental observations (Kim *et al.* 2014).

Combustion is modeled with the flamelet/progress-variable (FPV) approach (Pierce & Moin 2004; Ihme *et al.* 2005) in which the thermochemical properties are parameterize as a function of filtered mixture fraction $\tilde{Z}$, filtered reaction progress variable $\tilde{C}$ and mixture fraction variance. The progress variable is defined as (Ihme *et al.* 2012) $C = Y_{\mathrm{CO_2}} + Y_{\mathrm{CO}} + Y_{\mathrm{H_2O}} + Y_{\mathrm{H_2}}$. The flame structure is obtained from the solution of steady laminar non-premixed flamelet equations, which are solved along the entire S-shaped curve. Cooling effect of the liquid phase on the flamelet solution is considered by computing an effective gaseous fuel temperature (Moin & Apte 2006) $T_{fuel,g} = T_{fuel,l} - \Delta h_v(T_{evap})/c_{p,l}(T_{evap})$, where Δh_v is the latent heat of evaporation and $c_{p,l}$ is the specific heat capacity of the liquid.

3. Fuel description

The present study considers three fuels, namely a conventional petroleum-derived Jet-A fuel (Designation: Cat-A2, POSF 10325) and two test fuels: a fuel with a very narrow boiling characteristic (Cat-C5, POSF 12345) and a fuel with low cetane number (Cat-C1, POSF 11498). Key properties and composition of the three fuels are given in Table 1. Compared to Cat-A2, Cat-C5 and Cat-C1 have a similar and higher H/C ratio respectively. All three fuels differ in term of molecular weight where Cat-C5 is low than the conventional fuel while Cat-C1 is significantly higher.

Chemically, Cat-C5 has a significantly higher content of branched hydrocarbons and aromatics than Cat-A2, but has almost no cycloparaffins. Cat-C1 is composed only of *iso*-Paraffins with about 16% of highly branched-chain hydrocarbon (isocetane). The

	MW [kg/kmol]	H/C	LHV [MJ/kg]	Composition (mass fraction [%]) Aromatics	*iso*-Paraffins	*n*-Paraffins	Cycloparaffins
Cat-A2	159	1.90	43.1	18.66	29.45	20.03	31.86
Cat-C5	135	1.93	43.0	30.68	51.58	17.66	<0.001
Cat-C1	178	2.16	43.8	<0.001	99.63	<0.001	<0.001

TABLE 1. Properties of fuels studied.

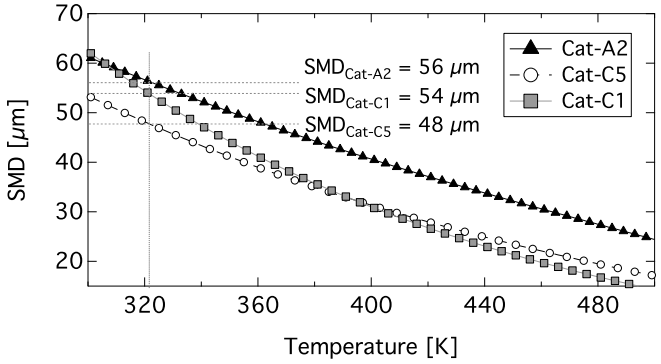

FIGURE 2. Comparison of injection SMD given by Lefebvre (1989) as function of liquid temperature.

physicochemical properties and combustion chemistry models for all fuels are obtained from studies conducted within the context of the National Jet Fuel Combustion Program (NJFCP) and implemented in the LES solver.

An *a-priori* analysis is performed to examine effects of fuel properties on droplet, combustion characteristics and LBO-behavior. Viscosity and surface tension of the liquid fuel affect the spray preparation during the primary and secondary breakup. To assess the effect of fuel properties on the spray characteristics we employ the dimensional correlation of Lefebvre (1989) for the Sauter mean diameter (SMD)

$$d_{SMD} = 2.25\sigma_L^{0.25}\mu_L^{0.25}\dot{m}_L^{0.25}\Delta P_L^{-0.5}\rho_{air}^{-0.25}, \tag{3.1}$$

where σ_L is the liquid surface tension, μ_L is the liquid viscosity, $\dot{m}_L$ is the liquid mass flow rate, ΔP_L is pressure drop across the injector nozzle and ρ_{air} is the surrounding gas density. The results are provided for both fuels as a function of temperature in Figure 2. In the conditions of the present study, the lower viscosity of the Cat-C5 results in a smaller SMD while Cat-C1 is very close to the reference fuel. Note that for higher injection temperature, Cat-C1 progressively diverges from Cat-A2, resulting in a lower SMD.

As the droplets are advected downstream, heat-transfer with the surrounding gas-phase leads to evaporation. The effect of the fuel properties is evaluated in an isolated 0D droplet evaporation code, where the evaporation time is computed for a range of initial droplet diameters and gas temperatures. Results for isolated droplets initially at 322 K in an environment at 2.07 atm and 1000 K are shown in Figure 3. This comparison shows that, compared to Cat-A2, the evaporation rate for the Cat-C5 is about 35% faster

[ht!]

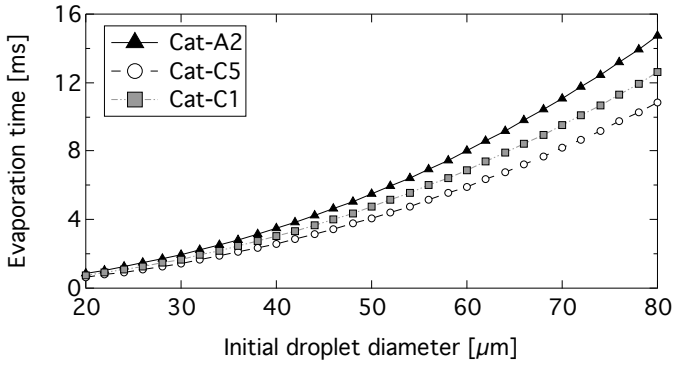

FIGURE 3. Comparison of evaporation time at various initial droplet diameter for a droplet initially at 322 K in a $P = 2.07$ atms and $T_g = 1000$ K environment.

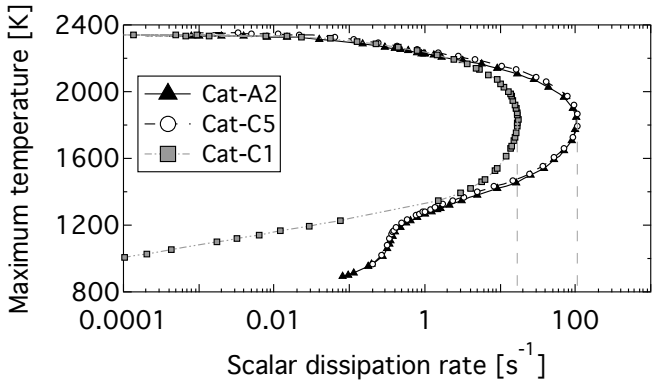

FIGURE 4. Comparison of maximum temperature in counterflow diffusion flamelets as function of scalar dissipation rate.

while the difference is only 16% for Cat-C1. Similar differences are observed over a [700 K-1400K] temperature range.

The combustion chemistry models are developed following a hybrid approach (Wang *et al.* 2015), in which fuel pyrolysis is described by six lumped reaction steps yielding primary pyrolysis products. The kinetics of these pyrolysis products are obtained from time-history data of shock tube and flow reactor studies. A foundational fuel chemistry model (USC Mech II) (Wang *et al.* 2010) is used to describe the oxidation kinetics of the pyrolysis products. By considering a counterflow diffusion flame configuration, relevant to the FPV-combustion model adopted in this study, chemical effects are evaluated by comparing the S-shaped curves for the three fuels as reported in Figure 4. Through this study, only marginal differences on the flamelet response to strain are evidenced between Cat-A2 and Cat-C5 where both fuels have an extinction scalar dissipation rate of $\chi_{ext} = 105$ s^{-1}. In contrast, a significant difference is observed between Cat-A2 and Cat-C1 with the extinction rate of the latter around $\chi_{ext} = 18$ s^{-1}.

In summary, the analysis indicates that the difference of physicochemical properties between the reference fuel Cat-A2 and the candidate test fuels primarily affects the physical processes and the chemical kinetics for Cat-C5 and Cat-C1, respectively.

	Effusion plates	Dilution holes		Swirler			
		Row 1	Row 2	Total	Radial	Axial int.	Axial ext.
Experiments	61.6	10.5	11.9	16.0	3.3	5.9	6.6
Simulation	58.3	10.9	11.9	18.9	3.6	6.3	9.0

TABLE 2. Comparison of measured and computed flow split [%] between swirler, effusion plates and dilution holes.

4. Results

LES-calculation of the referee-rig are performed with Cat-A2 and Cat-C5 at a stable operating point and during LBO triggered by fuel depletion. Before investigating the reactive flow in the referee combustor rig, statistics of velocity are collected from a non-reacting flow simulation during two flow-through-times in the primary zone and the flow split between the swirler, the dilution holes and the effusive plates is compared to experiments. Results are summarized in Table 2, showing that the LES is able to accurately reproduce the flow split between the primary zone and the secondary zone.

4.1. *Flow characteristics at stable operating condition*

The flow field showed in Figure 5 is typical for modern combustor designs where the strong swirl induced by the injection system results in a large inner recirculation zone (IRZ), which extends upstream within the injection system and interacts downstream with the first row of the dilution holes (highlighted in dark in Figure 5(a)). The flow-through-time in the primary zone (upstream of the first dilution row) is evaluated as 6 ms. The IRZ advects hot gases toward the injection nozzle acting as a strong flame stabilization mechanism, but the lack of pre-vaporized fuel and the high velocity within the injection system result in a lifted flame. The low boiling temperature of the Cat-C5 is found to allow evaporation within the injection system resulting in a global shift of the flame front toward the injector nozzle. The flame mostly lies in the shear layer between the hot recirculating gases of the IRZ and the incoming fresh gases where the droplet evaporation is enhanced by the flame temperature (as shown by the white iso-contour of heat release in Figure 5(a)). The flame is found to be significantly longer for the Cat-A2, with droplets penetrating further downstream in the primary zone as a result of the extended droplet life time. The temperature of the IRZ is much lower than the flame temperature due to the lean equivalence ratio of the primary zone ($\phi_{prim} = 0.18$) and the intermittent emission of fresh gases from the dilution holes.

The flame root, defined as the most upstream reacting flame front, undergoes a periodic oscillation due to the presence of the PVC. Because of the very low liquid mass flow rate near the LBO limit, the droplet injection velocity is low and droplets are rapidly entrained by the swirling air. The spray then interacts with the PVC forming clusters of droplets, which leads to a periodic variation of the evaporation rate. The PVC frequency, $f_{PVC} = 1056$ Hz, is evaluated using a probe (see cross in Figure 1) and this frequency is insensitive to the fuel or equivalence ratio.

4.2. *Lean blow-out*

Similarly to the experimental procedure, LBO is induced by progressive fuel depletion. However, the reduction of the fuel mass flow rate in the experiments extends over tens of seconds and a larger fuel reduction rate is adopted in the LES, owing to the computa-

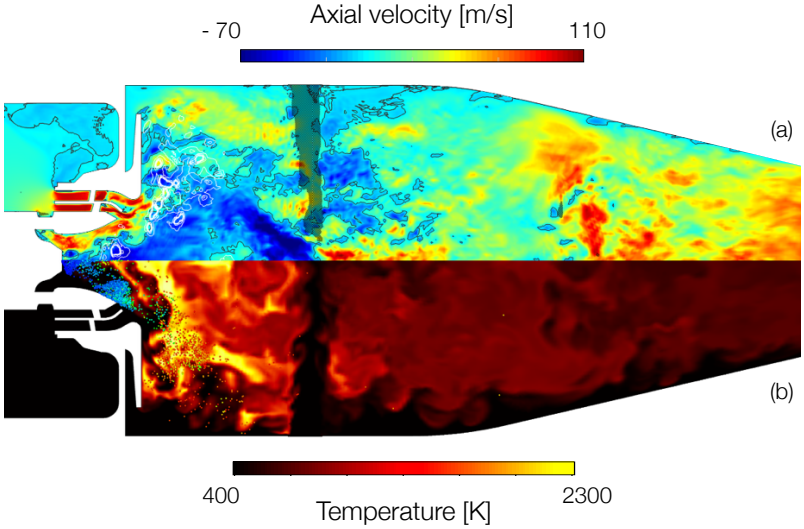

FIGURE 5. Axial velocity (a) and temperature field (b) in the combustion chamber x-normal central plane for Cat-A2 fuel. Superimposed on the velocity field are iso-contours of heat release (white) and the iso-contour of zero axial velocity (black). Droplets within a 1 mm slab around the central plane colored by their temperature are overlapped with the temperature field.

tional cost of the simulations. Over three flow-through-times in the primary zone of the combustor, the overall equivalence ratio is linearly decreased from $\phi = 0.1$ to $\phi = 0.07$ (corresponding to a rate of change of -45 g.s^{-2}). The latter is below the experimental LBO-limit for both fuels, but is used to ensure that LBO is triggered in the LES.

Figure 6 shows three instantaneous temperature fields in the combustor x-normal central plane along with droplets within a 1 mm slab around this plane for both Cat-A2 and Cat-C5. The first snapshots are taken shortly after the start of fuel ramping, so that the flame is not yet affected by the change in injection rate. Comparison between Cat-A2 and Cat-C5 highlights the fact that the latter flame is sitting closer to the injection system. As the fuel flow rate decreases, the temperature of the primary zone and in particular of the IRZ is decreased. It is found that the reduction of the averaged temperature in the IRZ slows the droplet heating and delays the evaporation, which reduces the gaseous fuel availability. Finally, complete extinction of the primary zone is illustrated for Cat-A2 in Figure 6(e) after 27 ms and the number of droplets in the combustion chamber progressively increase. The atypical flame structure shown in Figure 6(f) is observed close to blow-out where flame fronts are distributed throughout the primary zone but the flame is no longer stabilized at the injector nozzle.

To better characterize the transient evolution of the combustor state during blow-out, the temporal evolution of four key indicators is recorded: the total evaporation rate, the heat release integral, the mean temperature in the IRZ and the flame root distance from the pressure-swirl injector nozzle. The last two indicators are selected since experiments indicate that blow-out and its precursors are strongly related to the hot-gas recirculation (Muruganandam & Seitzman 2005; Stöhr *et al.* 2011). Results are plotted in Figure 7 and the injection rate is added on top of the evaporation rate. The latter is found to oscillate in stationary conditions due to the interaction of the spray with the PVC and similar oscillations are also observed at the flame root position. The LBO sequences can be split in three successive phases highlighted by the gray region in Figure 7:

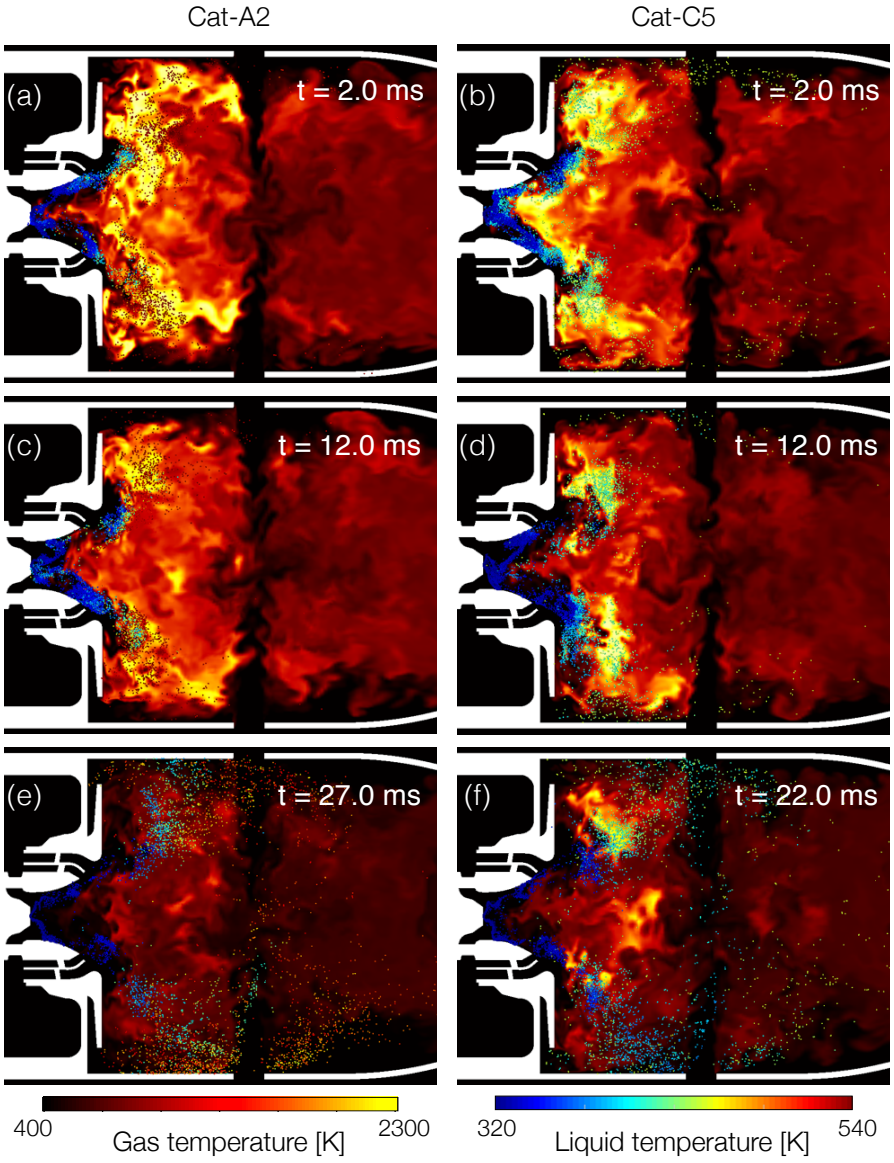

FIGURE 6. Instantaneous temperature fields in a x-normal central cut plane along with droplets colored by the liquid temperature at three instant after the start of fuel ramping for both Cat-A2 (left) and Cat-C5 (right). Time labels correspond to the time after the start of injection ramping.

- Initially, the combustor response to the change in injection rate exhibit an initial delay of 5 ms, corresponding to the residence time in the primary zone.
- Subsequently, the combustor response is characterized by a linear decrease of the evaporation rate, heat release and mean IRZ temperature while the flame root is progressively shifted downstream toward the primary zone. Both Cat-A2 and Cat-C5 are found to respond similarly. Note that due to strong oscillations of the stationary simulations, the small time advance of the Cat-C5 response is not considered to be an indication of its LBO behavior.

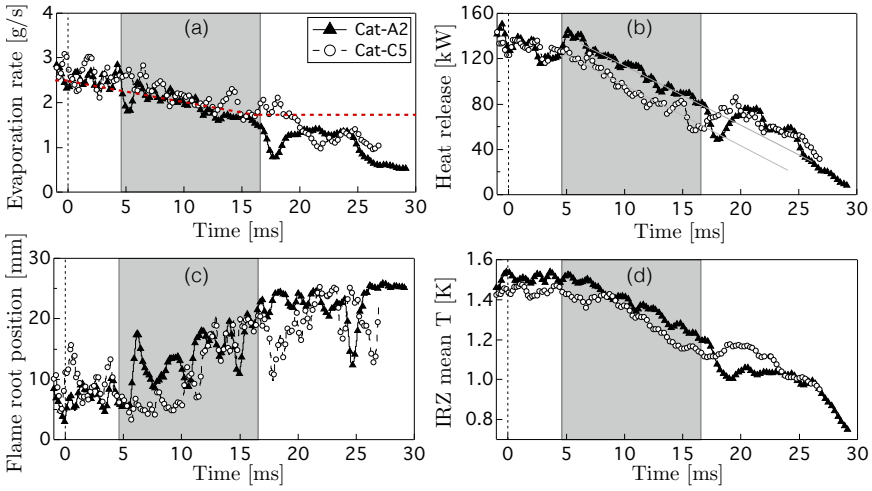

FIGURE 7. Temporal evolution of the total evaporation rate (a), heat release integral (b), flame root distance from the pressure-swirl nozzle (c) and mean IRZ temperature (d). Gray region corresponds to the linear change phase of the LBO sequence.

• Finally, after 16 ms, although the fuel injection rate is maintained at a constant value of 1.75 g/s ($\phi = 0.07$), the combustor exhibits large variations of the evaporation and heat release integral. This behavior is associated with partial recovery of the flame in the primary zone (Figure 6(f)), but the change in the IRZ temperature and position prevent the flame stabilization on the injector.

Overall, no significant differences are observed between Cat-A2 and Cat-C5 in terms of behavior during a LBO sequence. This result is in agreement with the experiments which show no substantial differences between the LBO-limit of the conventional Cat-A2 fuel and the Cat-C5 test fuel. The direct evaluation of the LBO-limit through LES is however difficult due to the long time scales of the experimental procedure.

5. Conclusions

The goal of the present study was to evaluate the LBO-behavior sensitivity to the fuel properties through LES. Besides a conventional Jet-A fuel, two test fuels were selected. Fuel effects on the relevant physicochemical processes were evaluated and have shown that the Cat-C5 test fuel primarily differs in terms of physical properties, while the Cat-C1 test fuel has a significantly lower chemical reactivity. Subsequently, LES of a LBO sequence was performed for two fuels (Cat-A2 and Cat-C5) and insignificant differences were observed between the LBO-behavior of the two fuels. This is in accordance with experimental observation. The flame blow-out is found to result from the weakening of the evaporation process induced by a change in the recirculating gas temperature and position. The fuel availability decreases, eventually leading to a complete extinction of the flame in the primary zone of the combustor.

Future work will include LES investigation of the Cat-C1 fuel, for which experimental data suggest an appreciable fuel effect on the LBO-limit. The analysis of the flame structure also indicates strong interactions between the spray and the flame front. Thus, the sensitivity of the results to the combustion modeling must be assessed and the development of accurate spray flamelet model will be investigated.

Acknowledgments

This work was funded by the US Federal Aviation Administration (FAA) Office of Environment and Energy as a part of ASCENT Project National Jet Fuel Combustion Program under FAA Award Number: 13-C-AJFE-SU-005. Any opinions, findings, and conclusions or recommendations expressed in this material are those of the authors and do not necessarily reflect the views of the FAA and ASCENT Sponsors. The authors gratefully acknowledge financial support from SAFRAN as well as Prof. H. Wang for providing the chemical mechanisms, Dr. T. Edwards for the physical properties of the fuels, Dr. N. Rizk for the spray correlation and Dr. V. Sankaran for the mesh generation.

REFERENCES

Apte, S., Gorokhovski, M. & Moin, P. 2003 LES of atomizing spray with stochastic modeling of secondary breakup. *Int. J. Multiphase Flow* **29** (9), 1503–1522.

Astm 2014 Standard practice for qualification and approval of new aviation turbine fuels and fuel additives. *Tech. Rep.* ASTM.

Ateshkadi, A., McDonel, V. & Samuelsen, G. S. 2000 Lean blowout model for a spray-fired swirl-stabilized combustor. *Proc. Comb. Inst.* **28**, 1281–1288.

Ballal, D. R. & Lefebvre, A. H. 1979 Ignition and flame quenching of flowing heterogeneous fuel-air mixtures. *Combust. Flame* **35**, 155–168.

Blakey, S., Rye, L. & Wilson, C. W. 2011 Aviation gas turbine alternative fuels: A review. *Proc. Comb. Inst.* **33** (2), 2863–2885.

Cavaliere, D., Kariuki, J. & Mastorakos, E. 2013 A comparison of the blow-off behaviour of swirl-stabilized premixed, non-premixed and spray flames. *Flow. Turbul. Combust.* **91**, 347–372.

Edwards, T. 2007 Advancements in gas turbine fuels from 1943 to 2005. *J. Eng. Gas Turb. Power* **129** (1), 13–20.

Esclapez, L., Riber, E. & Cuenot, B. 2015 Ignition probability of a partially premixed burner using LES. *Proc. Comb. Inst.* **35** (3), 3133–3141.

Feikema, D., Chen, R.-H. & Driscoll, J. 1990 Enhancement of flame blowout limits by the use of swirl. *Combust. Flame* **80** (2), 183–195.

Ihme, M., Cha, C. M. & Pitsch, H. 2005 Prediction of local extinction and re-ignition effects in non-premixed turbulent combustion using a flamelet/progress variable approach. *Proc. Combust. Inst.* **30**, 793–800.

Ihme, M., Shunn, L. & Zhang, J. 2012 Regularization of reaction progress variable for application to flamelet-based combustion models. *J. Comp. Phys.* **231**, 7715–7721.

Kim, D., Ham, F., Le, H., Herrman, M., Li, X., Soteriou, C. & Kim, W. 2014 High-fidelity simulation of atomization in a gas turbine injector high shear nozzle. In *ILASS Proceedings Americas 26th Liquid Atomization and Spray Systems*.

Lefebvre, A. H. 1985 Fuel effects on gas turbine combustion - ignition, stability, and combustion efficiency. *J. Eng. Gas Turb. Power* **105**, 24–37.

Lefebvre, A. H. 1989 Atomization and sprays, 1989. *Hemisphere, New York* .

Lieuwen, T., McDonell, V., Petersen, E. & Santavicca, D. 2008 Fuel flexibility influences on premixed combustor blowout, flashback, autoignition, and stability. *J. Eng. Gas Turb. Power* **130** (1), 011506.

Marinov, S., Kern, M., Zarzalis, N., Habisreuther, P., Peschiulli, A., Turrini, F. & Sara, O. N. 2012 Similarity issues of kerosene and methane confined

flames stabilized by swirl in regard to the weak extinction limit. *Flow. Turbul. Combust.* **89**, 73–95.

Maurice, L. Q., Lander, H., Edwards, T. & Harrison, W. 2001 Advanced aviation fuels: a look ahead via a historical perspective. *Fuel* **80** (5), 747–756.

Miller, R. S., Harstad, K. G. & Bellan, J. 2001 Direct numerical simulations of supercritical fluid mixing layers applied to heptane-nitrogen. *J. Fluid Mech.* **436**, 1–39.

Moin, P. & Apte, S. V. 2006 Large-eddy simulation of realistic gas turbine combustors. *AIAA J.* **44** (4), 698–708.

Moses, C. & Naegeli, D. 1979 Fuel property effects on combustor performance. In *ASME 1979 International Gas Turbine Conference and Exhibit and Solar Energy Conference*.

Muruganandam, T. & Seitzman, J. 2005 Origin of lean blowout precursors in swirled gas turbine combustors. *AIAA Paper* 2005-1163.

Pierce, C. D. & Moin, P. 2004 Progress-variable approach for large-eddy simulation of non-premixed turbulent combustion. *J. Fluid Mech.* **504**, 73–97.

Selle, L., Lartigue, G., Poinsot, T., Koch, R., Schildmacher, K.-U., Krebs, W., Prade, B., Kaufmann, P. & Veynante, D. 2004 Compressible large-eddy simulation of turbulent combustion in complex geometry on unstructured meshes. *Combust. Flame* **137** (4), 489–505.

Shanbhogue, S., Husain, S. & Lieuwen, T. 2009 Lean blowoff of bluff body stabilized flames: Scaling and dynamics. *Prog. Energy Comb. Sci.* **35**, 98–120.

Stohr, M., Boxx, I., Carter, C. & Meier, W. 2011 Dynamics of lean blowout of a swirl-stabilized flame in a gas turbine model combustor. *Proc. Comb. Inst.* **33**, 2953–2960..

Tyliszczak, A., Cavaliere, D. & Mastorakos, E. 2014 LES/CMC of blow-off in a liquid fueled swirl burner. *Flow. Turbul. Combust.* **92**, 237–267.

Vreman, A. W. 2004 An eddy-viscosity subgrid-scale model for turbulent shear flow: Algebraic theory and applications. *Phys. Fluids* **16** (3670).

Wang, H., Dames, E., Sirjean, B., Sheen, D. A., Tangko, R., Violi, A., Lai, J. Y. W., Egolfopoulos, F. N., Davidson, D. F., Hanson, R. K., Bowman, C. T., Law, C. K., Tsang, W., Cernansky, N. P., Miller, D. L. & Lindstedt, R. P. 2010 A high-temperature chemical kinetic model of n-alkane (up to n-dodecane), cyclohexane, and methyl-, ethyl-, n-propyl and n-butyl-cyclohexane oxidation at high temperatures.

Wang, H., Xu, R., Hanson, R., Davidson, D. & Bowman, C. 2015 A HyChem model of jet fuel combustion. Unpublished.